Effects of dust particle number on the structure and dynamics in a binary complex plasma system by Langevin dynamics simulation

Baoxia Li, Yang Liu, Xiaojiang Tang, Guannan Shi, Haoyu Qi, Xin Liu, Eric Robert, Feng Huang

Effects of dust particle number on the structure and dynamics in a binary complex plasma system by Langevin dynamics simulation ☆

Baoxia Li [a], Yang Liu [b], Xiaojiang Tang [a], Guannan Shi [a], Haoyu Qi [b], Xin Liu [a], Eric Robert [c], Feng Huang [b,c,d,*]

[a] College of Information and Electrical Engineering, China Agricultural University, Beijing 100083, China
[b] College of Science, China Agricultural University, Beijing 100083, China
[c] GREMI UMR7344, CNRS-Université d'Orléans, 14 rue d'Issoudun, BP6744, 45067 Orléans, France
[d] LE STUDIUM Loire Valley Institute for Advanced Studies, Centre-Val de Loire region, 45000 Orleans, France

Keywords:
Binary complex plasma
Structures and dynamics
Langevin dynamics simulation

A B S T R A C T

In this paper, Langevin dynamics simulation is used to study the influence of particle number on the structures and dynamics of a binary complex plasma, in which two kinds of particles with different masses are considered. The structures of the binary system are characterized by particle distribution, nearest-neighbor, and pair correlation function. The dynamics of the system are characterized by the evolution of average speed and kinetic energy as time, the mean square displacement (MSD) and self-diffusion coefficient of the binary particles. The lattice structures and the dynamics evolution of binary particles versus the particle number are investigated in detail in this paper. The space distribution shows that the binary particles easily fully separate themselves for a small particle number. The dynamics evolutions indicate that small particles reach the system center first, and then are pushed out by the later reached large particles. As the number of particles increases, the system becomes more ordered and the kinetic energy difference between the two kinds of particles becomes smaller. This study shows that the structure and dynamics of a binary complex plasma can be affected by dust particle number.

1. Introduction

Complex plasma consists of background plasma, neutral gas, and micrometer-sized grains, which widely exists in space [1–3], industrial plasma processing [4,5], fusion system [6] and laboratory plasma systems [7–9]. The charged particles suspended in plasma and their interaction with the background plasma make complex plasma exhibit some new physical phenomena in comparison with normal plasma and demonstrate their distinctive properties, such as strong coupling [10], collective mode and dust lattice wave [11–13], dust particle coagulation [14,15], special structure formed by different species of particles [16], diffusion and particle condensation behavior [17].

Complex plasma experimental studies have experienced remarkable growth with developing from initial ground experiments [18] to microgravity experimental [19], and from unitary (or monodisperse) dusty plasma systems to binary and polydisperse systems. Due to the addition of different particle species with different mass, charge, size, topological shape, particle number, etc., non-unitary systems will produce more complex phenomena than unitary systems, such as phase separation, different dynamics and spatial distribution of particles, different coagulation process, etc., the studies of which have certain application significance for dust particle coagulation growth process in plasma processing and the space detection influenced by dust particles. Binary system is the simplest non-unitary system, which contains two kinds of particle species. There are different ways to form binary systems with different properties. For example, the individual micro-particles pass through a strongly coupled particle system without affecting the structure of the penetrated particle cloud [20] and the passing particles and the strongly coupled particles with two sizes form the binary particle system. For different particles with the same mass-to-charge ratio despite having different mass and charge, they can mix together to form a binary system [21,22]. Chaudhuri et al. [23] used defocusing imaging technique to identify binary agglomerates (dimers) in complex plasmas, and found that unlike spherical particles, the defocused images of binary agglomerates showed distinct, stationary/periodically rotating interference fringe patterns. Du et al. [24] saw that the diffraction pattern of the

* Corresponding author at: College of Science, China Agricultural University, Beijing 100083, China.
E-mail address: huangfeng@cau.edu.cn (F. Huang).

https://doi.org/10.1016/j.cpc.2022.108612.

binary mixture exhibits isotropic concentric rings, typical for amorphous materials. The study of Wieben et al. [25] showed that the heat capacity exhibited excellent agreement with the Dulong-Petit law obtained from experiments and numerical simulation with different particle numbers, i.e. the heat capacity linearly increases as particles number. The dynamics under magnetic field of the binary Yukawa system showed that magnetic field provided an external control on the mobility ratio of the two kinds of particle species [26]. In microgravity experiments, the main structure features found in PKE-Nefedov included the stable and regular crystal structure along the vertical central axis, the central void with sharp boundary, and the vortices along horizontal axis and outer boundary [27]. The ion drag was considered as a key factor for void formation under microgravity conditions [28]. In the PK-3 plus, larger particles were added to the compression system initially with smaller particles, and then the large particles form an outer cloud that surrounds the smaller particles [29]. Based on fluorescent dust particles, Killer [30] studied the phase separation of binary dusty plasmas with 3% particle size differences in microgravity experiments, particle flux, density gradient and drift velocity at individual particle level can be measured.

Although the binary dusty plasmas have been studied in different situations [18–28], for a binary complex plasma, the features of the two species particles (such as, mass, charge, size, particle number, particle materials, etc.) and their distribution characteristics (separation or mixture) are the key impact factors on the system structures, dynamics, and the agglomeration growth process of dust particles. Among these factors, particle number has an important and direct impact on the study of particle growth, system structure and collective behavior, etc. However, how the particle number affects the phase separation and the dynamic process is still unclear and needs in-depth research. In this paper, the effects of particle number on the structure and dynamics of a binary complex plasma are investigated. This paper is organized as follows. In Sec. 2, the simulation system is introduced. In Sec. 3, simulation results are displayed and analyzed. In Sec. 4, the conclusion of the paper is summarized.

2. Simulation model

Langevin dynamic method is used in our simulation system, which brings the simulation closer to real complex plasma experiments by taking into account both the Brownian motion and damping effect self-consistently, and simplifies the simulation because no external thermostat is needed [31,32]. The Hamiltonian is defined as $H = K + U$, where K is the kinetic energy, and potential energy U is given as follows.

$$U = \sum_{i<j}^{N} U(r_{ij}) + \sum_{i=1}^{N} U_c(r_i). \tag{1}$$

In Eq. (1), $U(r_{ij}) = q^2[exp(-r_{ij}/\lambda_d) - \xi]/r_{ij}$ is the modified screened Coulomb interaction potential between particles i and j ($i, j = 1, 2 \ldots, N$) with considering the existence of interparticle attraction [33], where r_{ij} is the distance between particles i and j, λ_d is Debye length, and ξ is the attraction factor. $U_c(r_i) = m\omega^2 r_i^2/2$ is the quadratic confinement potential. ω and r_i denote the radial confinement frequency and the position of the particle i from the system center.

The force on a single particle is expressed as follows.

$$F = \sum_{i\neq j}^{N} F_{ij} + F_c + F_{ran} + f, \tag{2}$$

where $F_{ij} = -\partial U(r_{ij})/\partial r_{ij}$ is the interaction force between particles, $F_c = -\partial U_c/\partial r$ is the external confinement force from the trap holding the dust particle, $f = -m\mu dr/dt$ represents the friction force (μ is the friction coefficient), and F_{ran} is the source of random (thermal) motion of particles with a given kinetic temperature T [34].

Table 1
The value of parameters used in the simulation.

Parameters used in this simulation	Values of parameters
Charge of particles $\boldsymbol{q}$	1
Coefficient of friction $\boldsymbol{\mu}$	0.02
Temperature $\boldsymbol{T}$	0.001
Attraction coefficient $\boldsymbol{\xi}$	0.6
Mass of the particles $\boldsymbol{m}$	$m_a = 1$, $m_b = 4$
Restraint strength $\boldsymbol{\omega}$	0.1
Cut-off radius $\boldsymbol{r_c}$	12

In our simulation, two kinds of particles with the same charge (q) and the same number but different masses (m_a and m_b) are used, and the total number N of the dust particles in our system is variable. The two kinds of particles are evenly spaced in a simulation box of $L \times L$, in which $L = (N/n_d)^{1/2}$ and in this simulation we set the number density $n_d = 1$. The cut-off radius r_c is set as 12. The dimensionless unit of length is λ_d. Energy and time scale in our simulation are normalized by $E_0 = [\frac{m\omega_0^2}{2}(q^2)^2]^{\frac{1}{3}}$ and $t_0 = (m\lambda_d^3/q^2)^{1/2}$, respectively. The simulation time step is 0.02 t_0 and the total simulation time in this paper is 2000 t_0. Table 1 shows the specific parameters we used in the simulation.

For a dust particle system, the expression of the pair correlation function of particles is given by

$$g(r) = \frac{S}{N}\frac{N(r,\Delta)}{2\pi r\Delta}, \tag{3}$$

where S and N are the simulation area and the total dust particle number, $N(r, \Delta)$ represents the dust particle number in the range of $r - \Delta/2$ and $r + \Delta/2$ (in this simulation $\Delta = 0.1a$), and a is the average interparticle distance.

The mean squared displacement (MSD) of dust particles is given by

$$\langle R^2(t)\rangle = \left\langle \frac{1}{N}\sum_{i=1}^{N}\left(\vec{r}_i(t) - \vec{r}_i(0)\right)^2 \right\rangle, \tag{4}$$

where $\langle\cdots\rangle$ and $\vec{r}_i(t)$ respectively represent the thermal average and the position of ith particle at time t. The self-diffusion coefficient of dust particles is expressed as follows [35].

$$D = \lim_{t\to\infty}\frac{\langle R^2(t)\rangle}{4t}. \tag{5}$$

3. Simulation results and analysis

Fig. 1 shows the distribution of binary particles (a1)-(c1) and the lattice nearest-neighbor structures (a2)-(c2) for different particle number after the system reached a stable state (i.e. the macrostructure, particle distribution and dynamics of the whole system will no longer change significantly). From Fig. 1(a1) ($N = 64$), it can be seen that large particles are located in the system central region marked in red color, and the two particle species are clearly separated, i.e., no smaller particles are mixed into the large particle region. As the particle number increases, for example, at $N = 144$ (Fig. 1(b1)), it can be seen that six smaller particles mix in the large particles' region. When N increases to 256 (Fig. 1(c1)), the number of small particles mixed into the large particle area increases to 12. In addition, Fig. 1 shows that the system with more particles exhibits rounder boundary.

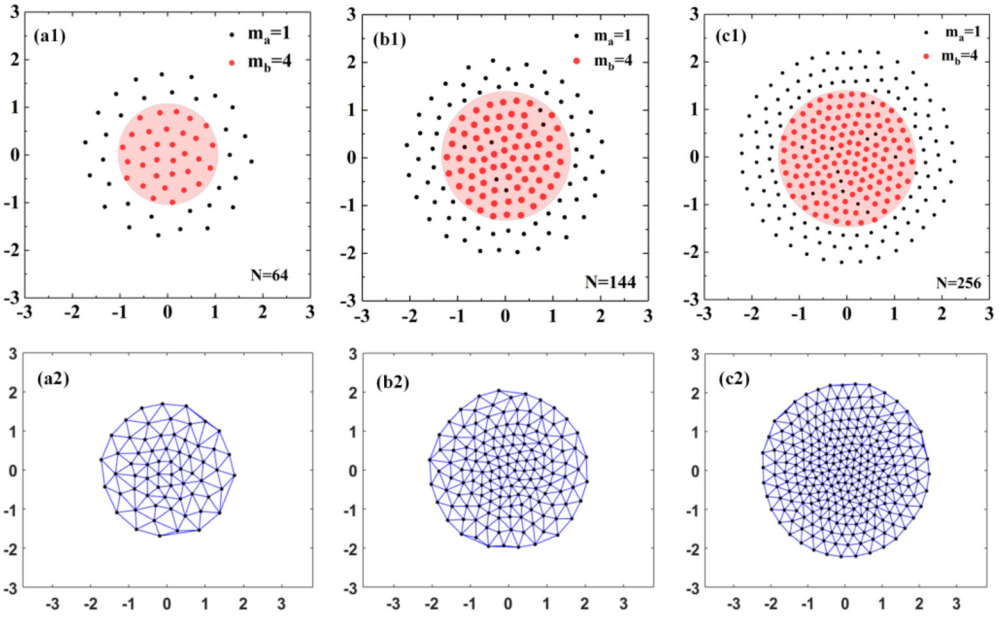

Fig. 1. The distribution of binary particles with different masses ($m_a = 1$ and $m_b = 4$) and the corresponding lattice nearest-neighbor structures. The red shaded areas, by drawing a circle using the coordinate (0, 0) as the center, are the distribution regions of large particles under different particle number. (For interpretation of the colors in the figure(s), the reader is referred to the web version of this article.)

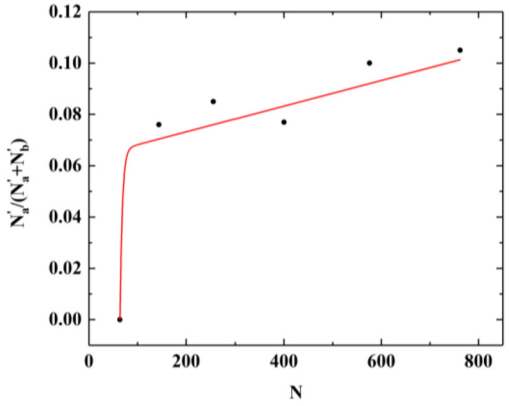

Fig. 2. The ratio $N'_a/(N'_a + N'_b)$ of smaller particles to all particles in the red shaded, documented in Fig. 1, evolution versus N. N'_a and N'_b represent the number of small and large particles in the red shaded area, respectively.

The hexagonal nearest-neighbor can be used to study the structure of a dust lattice in a 2D radial confinement system [36], i.e., more hexagonal structures represent a more ordered dust system. Fig. 1(a2-c2) shows the lattice structure connecting the nearest particles under different particle numbers. It is seen that hexagonal nearest-neighbor structure is dominant in such a system. When N increases from 64 to 144 and 256, the hexagon number (N'_h) gradually increases from 25 to 68 and 147 with more rounded outer boundary (Fig. 1(a2-c2)) and the ratio of N'_h/N increases from 0.39 to 0.47 and 0.57, as shown in Table 2, which indicates that for such a binary complex plasma system, larger particle number can produce more ordered lattice structures.

In order to study the specific particle distribution in the red area, Fig. 2 shows the fitted curve of $N'_a/(N'_a + N'_b)$ versus N, where N'_a and N'_b represent the number of small and large particles in the red shaded area, respectively. It is shown that when the particles number N is 64, $N'_a/(N'_a + N'_b)$ is 0, meaning the binary particles completely separated. When N reaches to 144, $N'_a/(N'_a + N'_b)$ suddenly increases from 0 to 0.076 and then slowly linearly increases in the range of $N < 800$. This shows that the probability of binary particles mixing together increases as N. In other words, smaller

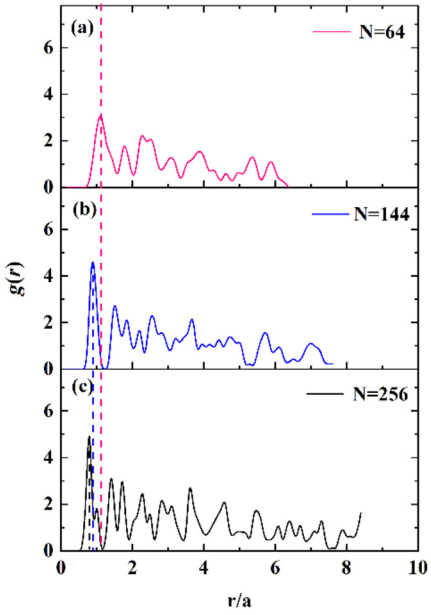

Fig. 3. The pair correlation functions with different particle number.

Table 2
N'_h and the ratio of N'_h/N with different N.

N	N'_h	N'_h/N
$N = 64$	25	0.39
$N = 144$	68	0.47
$N = 256$	147	0.57

N can promote more completely separation in binary systems, but with the less ordered lattice structure.

The pair correlation function $g(r)$ can also be used to characterize dust lattice structure. Fig. 3 shows the $g(r)$ curves for the binary lattice with different N. It shows that more and stronger

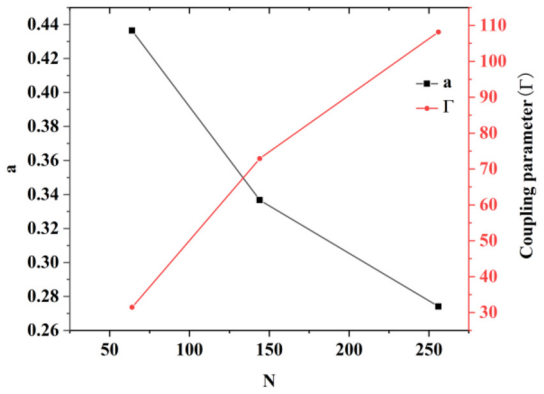

Fig. 4. The average interparticle distance (a) and the coupling parameter (Γ) versus N.

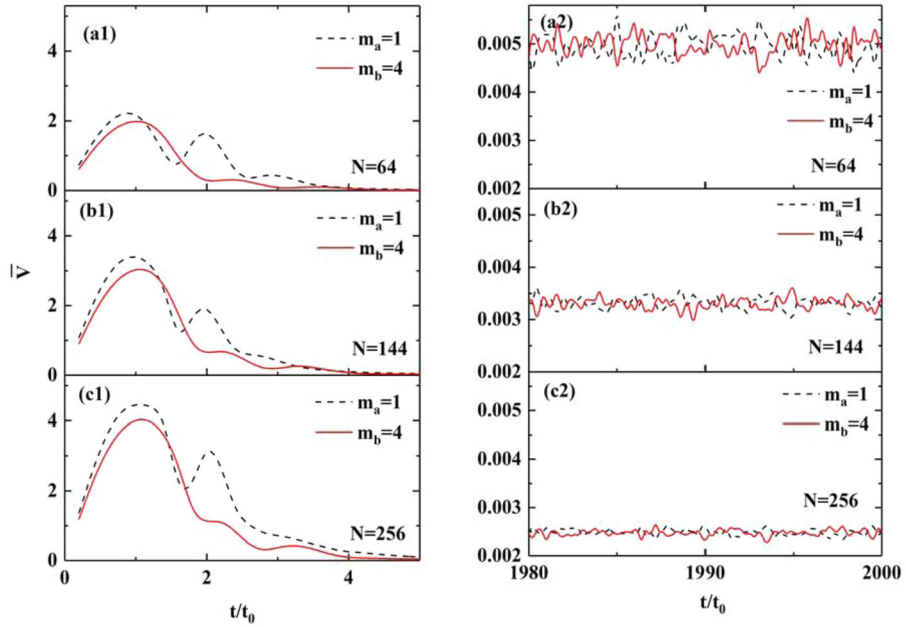

Fig. 5. The temporal evolution of average speed ($\overline{V}$) for different N.

peaks appear as N increases. Specifically, with the increase of N, the height of the first peak becomes stronger and at the same time its position gradually shifts to the left, and the double-peak in the second peak becomes more obvious. These results indicate as increasing N, the particles are getting closer and the probability of finding the nearest-neighbor particle increases, i.e. the binary lattice becomes more compact and more ordered.

After the system is stabilized, the average interparticle distance a and the coupling parameter $\Gamma(=q^2[exp(-a/\lambda_d)-\xi]/(akT))$ [34] versus N are shown in Fig. 4. It can be seen that as dust particle number increases, the interparticle distance a gradually decreases, and at the same time the coupling parameter Γ becomes stronger (e.g. as N increases from 64 to 256, a decreases from 0.436 to 0.274 and Γ increases from 31.471 to 108.15), meaning the lattice becomes more compact and the interparticle coupling stronger, which is in agreement with the result of Fig. 3.

The dynamic characteristics of the binary dust lattice can be investigated by the temporal evolution of the average speed of particles. Fig. 5(a1)-(c1) represent the evolution of the average speed of binary particles with different N in $t = 0$–5. It shows that at the initial stage of evolution, two kinds of particles exhibit different evolution curves. Taking $N = 256$ as an example, it is seen that the first peaks of binary particles both appear at about $t = 1$, mainly due to the acceleration toward the system center driven by the radial confinement. Small particles ($m_a = 1$) will reach the system center earlier (at $t = 1.6$, the valley in dash curve) and then are pushed out mainly by the large particles later reaching the center, causing the second peaks of the dash curve (at $t = 2$) with the weaker intensity than its first peak. The much weaker second peak on the solid curve is due to the slightly increased speed caused by the repulsion between large particles gathering in the center.

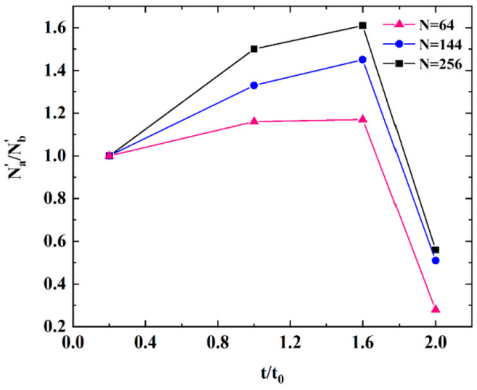

Fig. 6. The ratio of small and larger particles (N'_a/N'_b) in the red region temporal evolution during $t = 0$–2.

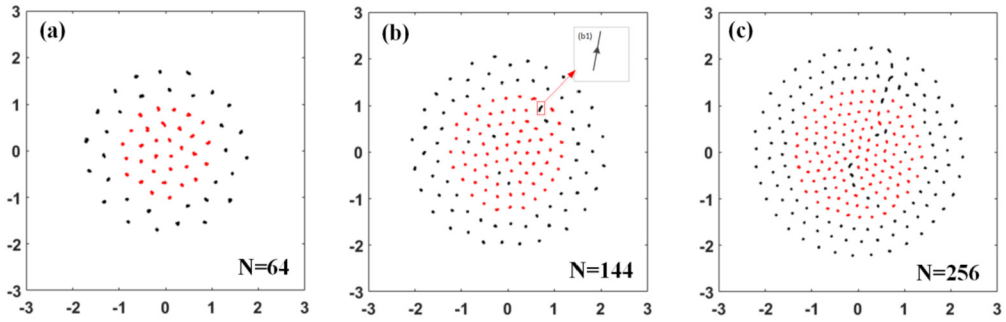

Fig. 7. The trajectories of all particles with different N at $t = 1800$–2000 (the colors of large and small particles are represented by red and black, respectively). The subfigure (b1) shows the enlarged trajectory of a small particle mixed in the large particle area with the arrow representing the direction from the initial to the final position.

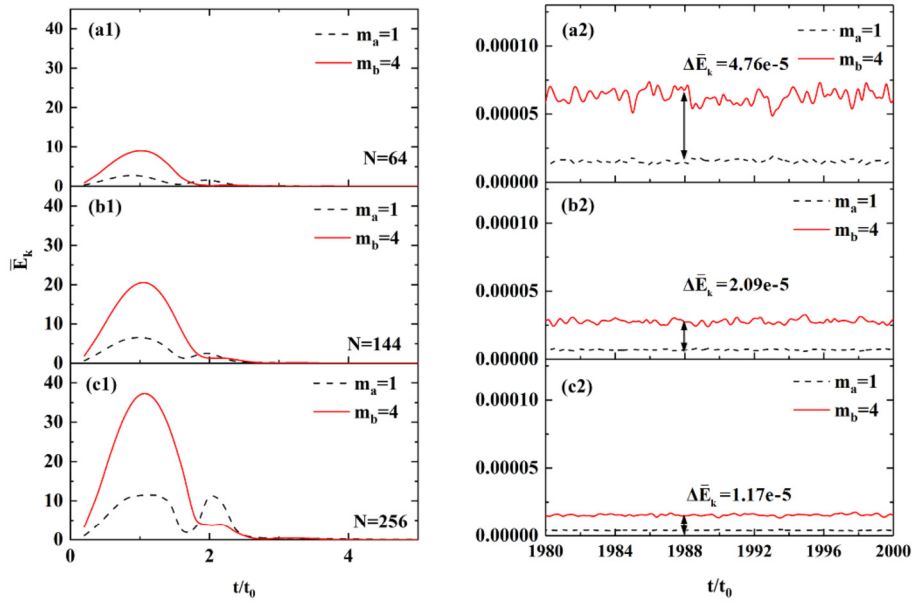

Fig. 8. The temporal evolution of average kinetic energy ($\overline{E}_k$) for different N.

In addition, from Fig. 5(a1)-(c1) it is obviously shown that as N increases, the peak intensity of binary particles becomes stronger at the initial stage of evolution. Fig. 5(a2)-(c2) represent the average speed of binary particles after the system reaches the steady state during 1980–2000 t_0. One can see that for a given value of N, the respective average speed evolution curves of binary particles fluctuate around a certain value, and with the increase of N from 64 to 256, the average speed decreases from 0.005 to 0.0025. The long-term fluctuation of the speed is less pronounced as N increases, probably revealing a more efficient thermalization of the binary lattice.

From Fig. 5, it is already shown that at the initial stage of the evolution ($t = 0$–2), the speed curves of both the two kinds of particles experience the most violent and complex changes with the process of small particles gathering to the center first and then being pushed out. Thus, in the fixed red region (marked in Fig. 1) the number ratio of the two kinds of particles also experiences the complex evolution. Fig. 6 shows the temporal evolution of the ratio of N'_a/N'_b in the marked region during $t = 0$–2. It is seen that for a certain N, N'_a/N'_b increases first and then decreases (e.g. at $N = 64$ and $t = 0.2$, 1.6 and 2, N'_a/N'_b increases from 1 to 1.17 and then reduces to 0.28). In addition, N'_a/N'_b increases as N, except $N'_a/N'_b = 1$ at the beginning of evolution (for example, $t = 0.2$), which is due to the evenly spaced initial arrangement of the two kinds of particles in the simulation box of $L \times L$. These results indicate that with the evolution of time, the less N, the less the ratio of N'_a/N'_b. That is, the binary particles with smaller N are quicker to be completely separated. Or, the more particles, the easier it is to produce mixing phase.

In the mixing phase, the individual small particles still have the trend to be slowly pushed out from the mixture region even when the system is considered to reach stable state. Fig. 7 shows trajectories of two kinds of particles after the system is steady within $t = 1800$–2000. It shows that most of particles oscillate near their equilibrium positions, and only the few smaller particles have the trend to be pushed outward from the mixture region (Fig. 7(b) and (c)). The subfigure (Fig. 7(b1)) shows the enlarged trajectory of a small particle in the mixture region indicating its trend of being pushed out when the system is considered as steady.

The temporal evolution of kinetic energy can also be used to characterize the dynamical behavior in such a binary system, as shown in Fig. 8. From Fig. 8(a1)-(c1), it can be seen that in the initial evolution process, the first peaks of the $\overline{E}_k - t$ curve for large and smaller particles both appear at about $t = 1$ and the peaks of large particles are stronger than the smaller particles due to their larger mass. The two peaks of small particles and the change trend with N are almost in agreement with Fig. 5. In addition, it is seen that in such a radial confinement system, $\overline{E}_k$ of both the binary particles quickly decays to a very low value after $t = 3$. Fig. 8(a2)-(c2) show the temporal evolution of $\Delta\overline{E}_k$ with N after the system reached the steady state. It shows that at a certain N, the kinetic energy of large particles is larger than the smaller ones (e.g. at

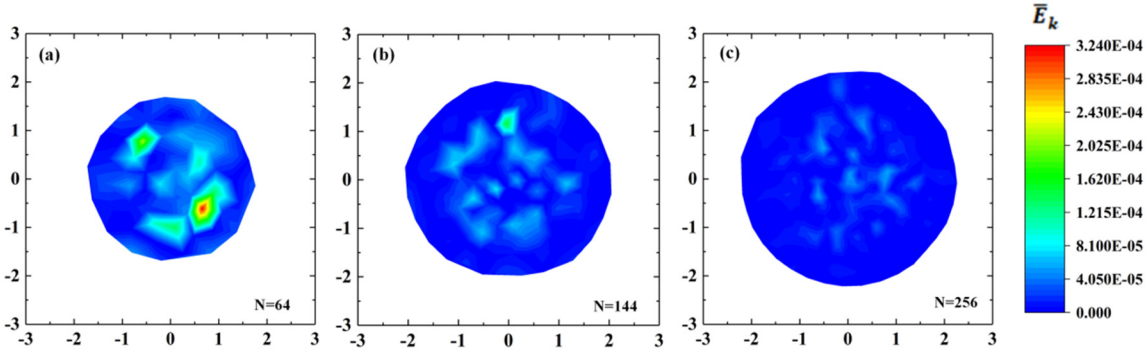

Fig. 9. The space distribution of kinetic energy when the system reaches steady state.

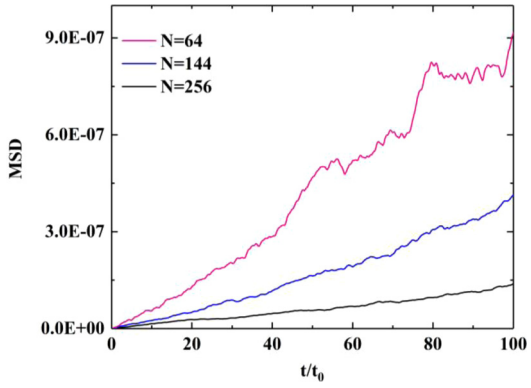

Fig. 10. The MSD of the system for different N after the system reached the steady state.

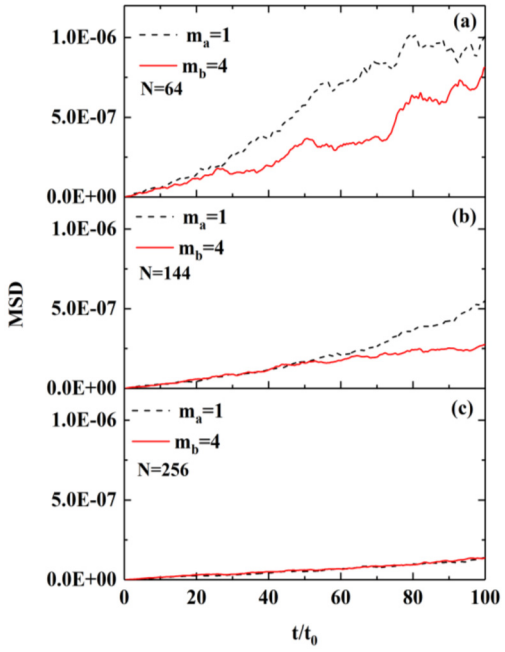

Fig. 11. The MSD of binary particles for different N after the system reached the steady state.

$N = 256$, $\overline{E}_{kb}$ and $\overline{E}_{ka}$ is 1.67×10^{-5} and 3.84×10^{-6}, respectively). As N increases, $\Delta\overline{E}_k$ becomes smaller (for example, as N increases from 64 to 256, $\Delta\overline{E}_k$ decrease from 4.76×10^{-5} to 1.17×10^{-5}) and at the same time the fluctuation of the $\overline{E}_k - t$ curve weakens.

When the system reaches steady state, the space distribution of kinetic energy is shown in Fig. 9 (the color represents the magnitude of kinetic energy). At $N = 64$, the obvious spatial distribution of color from the internal to outer region indicates the obvious difference in spatial distribution of thermal kinetic energy. With the increase of N, the color difference between the internal and outer regions (with radial distribution characteristics) decreases gradually. At $N = 256$, the whole blue distribution represents the lower kinetic energy. In addition, when N increases from 64 to 256, the difference between the average kinetic energy of particles in the red shaded area and its surrounding area $\Delta\overline{E}_k$ decreases from 4.44×10^{-5} to 1.13×10^{-5}.

The mean square displacements (MSD) and self-diffusion coefficients (D) [35] can also be used to study the dynamical characteristics of such a binary particle system. Fig. 10 and Fig. 11 show the MSD curves of the whole system and the individual curves of the two kinds of particles. From Fig. 10, one can see that as N increases, the MSD of the whole system gradually decreases, indicating the particle movement weakens. When N increases to 256, the low MSD value (e.g. 1.40×10^{-9} at $t = 2000$) shows a solid-like state with the dust particles only vibrating around their equilibrium positions [37]. From Fig. 11, it is seen that for a certain N the MSD curves of the two kinds of particles gradually separate as time going on, and the MSD of the smaller particles is larger than that of larger particles. Fig. 11 also shows that as the increase of N, the MSD curves of the two kinds of particles gradually approach each other, i.e. more particle number will decrease the dynamic difference between the two kinds of particles and promote the system dynamic uniformity.

The self-diffusion coefficient D can be obtained according to Eq. (5) [35], and is shown in Fig. 12. Fig. 12(a) shows that the self-diffusion coefficient of the whole system decreases as number N increases, Fig. 12(b) shows that the self-diffusion coefficient of smaller particles is larger (e.g. at $N = 64$, the self-diffusion coefficients of smaller and larger particles are 1.02×10^{-7} and 8.12×10^{-8}, respectively), which indicates that the stronger diffusion ability of smaller particles. In addition, both the self-diffusion coefficients of the two kinds of particles decrease as N, and the weaker diffusion ability at higher N indicates the more ordered and stable structure, which is in agreement with the results of Fig. 1, Fig. 3 and Fig. 4.

For the simulation in this paper, the binary particles are assumed to have the same charges but with different masses. In the ground experiments, due to the non-negligible influence of gravity, in order to make particles of different masses suspended in the same height to form a 2D or quasi 2D system, the sheath structures need to be designed accordingly. In microgravity, it's easier to implement that particles of different masses are suspended at the same height to form a 2D system. Thus, the assumption of this simulation is naturally applicable to microgravity situation. During this simulation, the applied inward strong confinement and the attraction between particles make the binary particles of initial uniform mixing quickly distribute themselves into two separated regions to form the minimum-energy configuration or steady-state

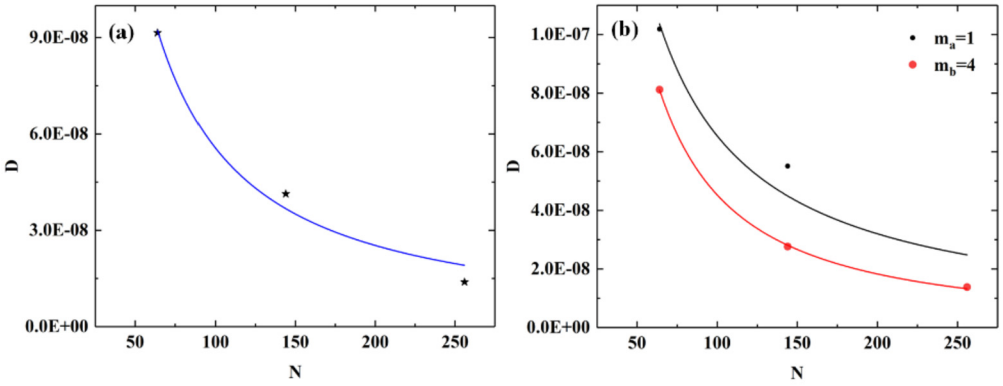

Fig. 12. The self-diffusion constant D of (a) the total system and (b) two kinds of particles for different N.

configuration, which is closely related to the specific form of system potential, kinetic energy, and parameters of particle species.

4. Conclusions

In this paper, we use Langevin dynamic method to investigate the effect of particle number on structures and dynamics characteristics in a radial confinement binary complex plasma system. From the results of the distribution of particles, lattice structure and pair correlation function, it can be seen that as dust particle number increases, the system becomes more compact and orderly, and coupling parameter gradually increases. The particle number also has the influence on the separation phase and dynamical evolution in such a binary system. It shows that smaller particles reach the center of the system at first and then pushed out mainly by the later reached large particles. As the increase of particle number, the difference of kinetic energy between the two kinds of particles gradually decreases, the MSD and self-diffusion coefficient are gradually weakened. This study is helpful for the application of phase separation in practical plasma environment related to different particle species.

Declaration of competing interest

We declare that we have no known competing financial interests or personal relationships that could have appeared to influence the work reported in this paper.

Data availability

The authors do not have permission to share data.

Acknowledgements

This work is supported by the National Natural Science Foundation of China (No. 12075315 and 11675261).

References

[1] S. Dyadechkin, E. Kallio, P. Wurz, J. Geophys. Res. Space Phys. 120 (2015) 1589–1606, https://doi.org/10.1002/2014JA020511.
[2] N. Meyer-Vernet, M. Moncuquet, K. Issautier, P. Schippers, J. Geophys. Res. Space Phys. 122 (2017) 8–22, https://doi.org/10.1002/2016JA023081.
[3] D.A. Mendis, M. Rosenberg, IEEE Trans. Plasma Sci. 20 (1992) 929–934, https://doi.org/10.1109/27.199553.
[4] J.F. Daviet, L. Peccoud, F. Mondon, J. Appl. Phys. 73 (1993) 1471–1479, https://doi.org/10.1063/1.353221.
[5] K. Karahashi, S. Hamaguchi, J. Phys. D, Appl. Phys. 47 (2014) 224008, https://doi.org/10.1088/0022-3727/47/22/224008.
[6] J. Winter, Plasma Phys. Control. Fusion 40 (1998) 1201–1210, https://doi.org/10.1088/0741-3335/40/6/022.
[7] P.K. Shukla, B. Eliasson, Rev. Mod. Phys. 81 (2009) 25–44, https://doi.org/10.1103/RevModPhys.81.25.
[8] M.S. Alam, M.M. Masud, A.A. Mamun, Astrophys. Space Sci. 349 (2014) 245–253, https://doi.org/10.1007/s10509-013-1639-3.
[9] S.N. Antipov, M.M. Vasiliev, M.M. Alyapyshev, O.F. Petrov, V.E. Fortov, J. Phys. Conf. Ser. 511 (2014) 012008, https://doi.org/10.1088/1742-6596/511/1/012008.
[10] M. Rosenberg, G. Kalman, Phys. Rev. E 56 (1997) 7166–7173, https://doi.org/10.1103/physreve.56.7166.
[11] M. Rosenberg, G. Kalman, AIP Conf. Proc. 446 (1998) 135–141, https://doi.org/10.1063/1.56661.
[12] A.A. Mamun, P.K. Shukla, Phys. Lett. A 373 (2009) 3161–3164, https://doi.org/10.1016/j.physleta.2009.06.052.
[13] G.J. Kalman, P. Hartmann, Z. Donkó, K.I. Golden, S. Kyrkos, Phys. Rev. E 87 (2013) 043103, https://doi.org/10.1103/PhysRevE.87.043103.
[14] Y. Liu, H.Y. Tang, X.J. Tang, Y.H. Liu, F. Huang, IEEE Trans. Plasma Sci. 48 (2020) 1173–1176, https://doi.org/10.1109/tps.2020.2981345.
[15] S.Z. Jiang, X.N. Hou, J. Kong, L.S. Matthews, T.W. Hyde, F. Huang, M.J. Wang, Chin. Phys. Lett. 35 (2018) 125201, https://doi.org/10.1088/0256-307x/35/12/125201.
[16] P. Hartmann, Z. Donko, G.J. Kalman, S. Kyrkos, K.I. Golden, M. Rosenberg, Phys. Rev. Lett. 103 (2009) 245002, https://doi.org/10.1103/PhysRevLett.103.245002.
[17] O.S. Vaulina, S.V. Vladimirov, Phys. Plasmas 9 (2002) 835–840, https://doi.org/10.1063/1.1449888.
[18] K. Mangold, J. Birk, P. Leiderer, C. Bechinger, Phys. Chem. Chem. Phys. 6 (2004) 1623–1626, https://doi.org/10.1039/B312966G.
[19] K. Jiang, L.J. Hou, A.V. Ivlev, Y.F. Li, K.R. Sütterlin, H.M. Thomas, G.E. Morfill, IEEE Trans. Plasma Sci. 39 (2011) 2752–2753, https://doi.org/10.1109/tps.2011.2153878.
[20] G.E. Morfill, U. Konopka, M. Kretschmer, M. Rubin-Zuzic, H.M. Thomas, S.K. Zhdanov, V. Tsytovich, New J. Phys. 8 (2006) 7, https://doi.org/10.1088/1367-2630/8/1/007.
[21] Y.H. Liu, L.Y. Chew, J. Phys. Condens. Matter 19 (2007) 356213, https://doi.org/10.1088/0953-8984/19/35/356213.
[22] Y.H. Liu, Z.Y. Chen, M.Y. Yu, L. Wang, A. Bogaerts, Phys. Rev. E 73 (2006) 047402, https://doi.org/10.1103/PhysRevE.73.047402.
[23] M. Chaudhuri, V. Nosenko, C. Knapek, U. Konopka, A.V. Ivlev, H.M. Thomas, G.E. Morfill, Appl. Phys. Lett. 100 (2012) 264101, https://doi.org/10.1063/1.4729755.
[24] C.R. Du, V. Nosenko, H.M. Thomas, Y.F. Lin, G.E. Morfill, A.V. Ivlev, Phys. Rev. Lett. 123 (2019) 185002, https://doi.org/10.1103/PhysRevLett.123.185002.
[25] F. Wieben, D. Block, Phys. Rev. Lett. 123 (2019) 225001, https://doi.org/10.1103/PhysRevLett.123.225001.
[26] T. Ott, H. Löwen, M. Bonitz, Phys. Rev. E 89 (2014) 013105, https://doi.org/10.1103/PhysRevE.89.013105.
[27] A.P. Nefedov, G.E. Morfill, V.E. Fortov, et al., New J. Phys. 5 (2003) 33, https://doi.org/10.1088/1367-2630/5/1/333.
[28] M. Kretschmer, S.A. Khrapak, S.K. Zhdanov, H.M. Thomas, G.E. Morfill, V.E. Fortov, A.M. Lipaev, V.I. Molotkov, A.I. Ivanov, M.V. Turin, Phys. Rev. E 71 (2005) 056401, https://doi.org/10.1103/PhysRevE.71.056401.
[29] A.G. Khrapak, V.I. Molotkov, A.M. Lipaev, D.I. Zhukhovitskii, V.N. Naumkin, V.E. Fortov, O.F. Petrov, H.M. Thomas, S.A. Khrapak, P. Huber, A. Ivlev, G. Morfill, Contrib. Plasma Phys. 56 (2016) 253–262, https://doi.org/10.1002/ctpp.201500102.
[30] C. Killer, T. Bockwoldt, S. Schütt, M. Himpel, A. Melzer, A. Piel, Phys. Rev. Lett. 116 (2016) 115002, https://doi.org/10.1103/PhysRevLett.116.115002.
[31] T.S. Ramazanov, K.N. Dzhumagulova, S.K. Kodanova, T.T. Daniyarov, M.K. Dosbolayev, Contrib. Plasma Phys. 49 (2009) 15–20, https://doi.org/10.1002/ctpp.200910003.

[32] M.N. Kadijani, H. Abbasi, Phys. Plasmas 23 (2016) 093707, https://doi.org/10.1063/1.4962689.
[33] F. Huang, Y.H. Liu, M.F. Ye, X.J. Wang, L. Wang, Chin. Phys. Lett. 27 (2010) 115201, https://doi.org/10.1088/0256-307X/27/11/115201.
[34] Y. Liu, X. Zhu, Y. Wang, Z. Chen, F. Huang, Contrib. Plasma Phys. 60 (2020) 201900190, https://doi.org/10.1002/ctpp.201900190.
[35] Y.L. Song, Y.F. He, F. Huang, Y.H. Liu, Z.Y. Chen, L. Wu, M.Y. Yu, Phys. Plasmas 22 (2015) 063702, https://doi.org/10.1063/1.4922436.
[36] Y.H. Liu, L.Y. Chew, M.Y. Yu, Phys. Rev. E 78 (2008) 066405, https://doi.org/10.1103/PhysRevE.78.066405.
[37] Y.L. Song, F. Huang, Z.Y. Chen, Y.H. Liu, M.Y. Yu, Phys. Lett. A 380 (2016) 886–895, https://doi.org/10.1016/j.physleta.2015.12.028.